

Foiling Normal Patterns of Crystallization by Design. Polymorphism of Phosphangulene Chalcogenides

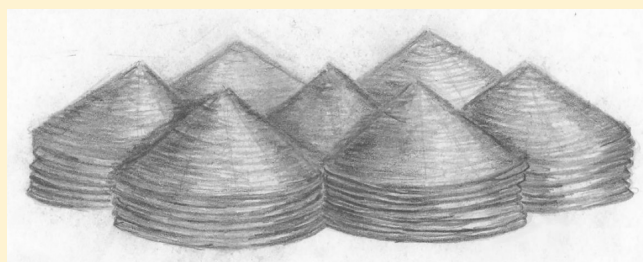
Published as part of a *Crystal Growth and Design virtual special issue Remembering the Contributions and Life of Prof. Joel Bernstein*

Alice Heskia, Thierry Maris,^{ib} and James D. Wuest*^{ib}

Département de Chimie, Université de Montréal, Montréal, Québec H3C 3J7 Canada

S Supporting Information

ABSTRACT: Phosphangulene (**1**) has a well-defined hexacyclic structure with a distinctive conical shape and an electron-rich aromatic surface. Molecules of phosphangulene are disposed to crystallize in parallel π -stacks. This preference can be thwarted by adding a single atom and converting phosphangulene into the corresponding oxide (**2a**), sulfide (**2b**), and selenide (**2c**). This change creates an awkward molecular shape that prevents effective stacking. As a consequence, the formation of optimal intermolecular interactions is inhibited, and multiple polymorphs with high values of Z and Z' are formed. The high polymorphism of chalcogenides **2a–c** is particularly noteworthy because the compounds have little flexibility. Analysis of the structures of phosphangulene, chalcogenides **2a–c**, and related compounds provides deeper understanding of crystallization, including how to design molecules that cannot pack efficiently, are unable to achieve normal patterns of association, and are therefore predisposed to form multiple polymorphs, structures with high values of Z and Z' , solvates, solid solutions, and cocrystals.



INTRODUCTION

Phosphangulene (**1**) has a characteristic conical shape reminiscent of traditional hats worn in parts of Asia (Figure 1). The compound was first reported by Krebs and co-workers,

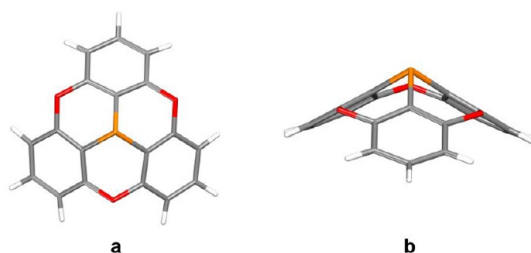
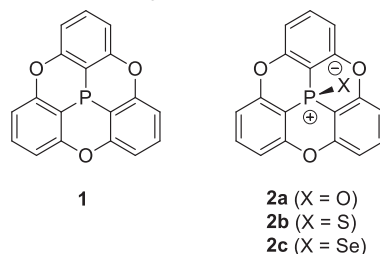


Figure 1. (a, b) Representations of the molecular structure of phosphangulene (**1**) in crystals grown from ethyl acetate, as viewed along the C_3 axis and perpendicular to the axis. Atoms of carbon appear in gray, hydrogen in white, oxygen in red, and phosphorus in orange.

who determined the structure of crystals grown from ethyl acetate.¹ The nonplanarity of phosphangulene gives rise to a dipole moment, determined to be 3.3 ± 0.2 D in CHCl_3 ,¹ which is slightly larger than the moment of triphenylphosphine (1.49 D in benzene).^{2,3} On the basis of ab initio calculations and multipolar modeling of X-ray structure factors, the direction of the dipole in phosphangulene is considered to

run along the C_3 axis from the apex of the cone (with the atom of phosphorus at the negative end) toward the base (with the peripheral atoms of hydrogen at the positive end).⁴



In crystals of phosphangulene, topology works in harmony with polarity to control molecular packing, which yields π -stacks with dipole moments aligned in parallel (Figure 2a). No other polymorph has been reported. Each stack is linked to six neighboring stacks by short C–H...O interactions (2.395 Å), as shown in Figure 2. Unexpectedly, the dipole moments of neighboring stacks point in the same direction, thereby yielding $R3m$ crystals that are polar and pyroelectric. Temporary voltages are generated when pyroelectric materials are heated or cooled, making them suitable for use in high-performance infrared detectors and other devices. Pyroelectric

Received: July 11, 2019

Revised: August 3, 2019

Published: August 6, 2019

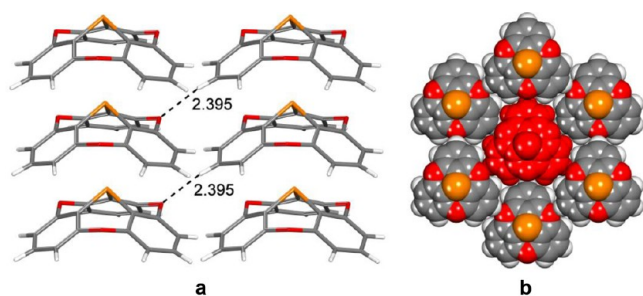


Figure 2. Representations of the structure of crystals of phosphangulene grown from ethyl acetate. (a) View perpendicular to the c -axis, showing part of two adjacent π -stacks with aligned dipoles. Principal interstack C–H \cdots O interactions are marked by broken lines, with distances given in Å. (b) View along the c -axis, showing how a central stack (in red) is surrounded by six others. Unless otherwise indicated, atoms are shown in standard colors.

carbon-based materials are uncommon, and their characteristically low densities and small dielectric constants give them advantages not normally shared by inorganic materials. As a consequence, phosphangulene and its derivatives define a structurally intriguing family of compounds with significant potential utility.

Key features in the structure of phosphangulene can be highlighted by Hirshfeld surfaces of molecules in the crystal and by the corresponding two-dimensional fingerprint plots.^{5,6} Hirshfeld surfaces are typically constructed to show the locus of points around a molecule in a crystal where the calculated electron density contributed by the molecule equals that contributed by all other atoms in the structure. The convex and concave surfaces of phosphangulene are shown in Figure 3.

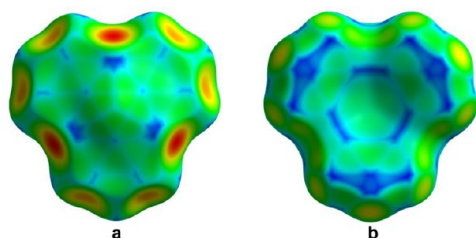


Figure 3. (a) Hirshfeld surface of the convex face of a molecule of phosphangulene in crystals grown from ethyl acetate. The surface is colored according to the local value of d_e (distance from the surface to the nearest atomic nucleus in another molecule), and the colors range from cool (blue) to hot (red) as d_e decreases. (b) Corresponding surface of the concave face.

The surfaces are colored according to the local value of d_e , which is the distance from the surface to the nearest atomic nucleus in another molecule, and the colors vary from cool (blue) to hot (red) as d_e decreases. Figure 3 underscores several key features, including (1) the C_{3v} molecular symmetry of phosphangulene, (2) the presence of six significant C–H \cdots O interactions per molecule, denoted by conspicuous red spots located on the convex surface near each atom of oxygen, and (3) the weak affinity of the convex and concave π -surfaces, as indicated by the high proportion of blue and green around the center of each molecule. The primary driving forces for stacking appear to be topology and dipolar alignment rather than π – π interactions, and stacked molecules are separated by a relatively long distance (4.259 Å), which corresponds to the length of the unit cell along the c -axis.

The fingerprint plot in Figure 4 provides complementary information by showing the frequency of finding points on the

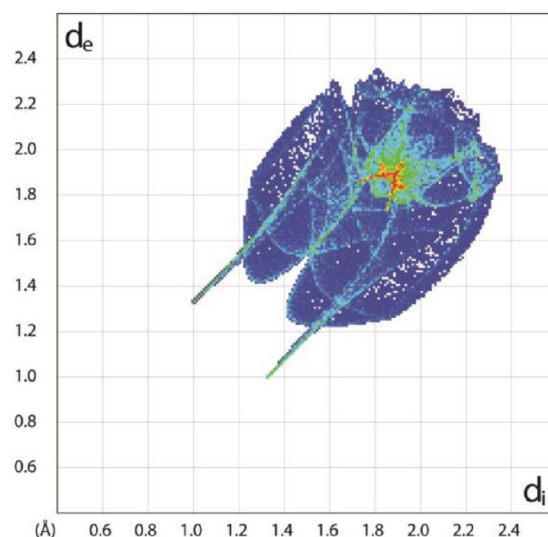


Figure 4. Two-dimensional fingerprint plot of the Hirshfeld surface for molecules of phosphangulene in crystals grown from ethyl acetate. The plot shows the frequency of finding points on the surface with particular values of d_e and d_i (distances to the nearest external and internal atomic nuclei). The colors at each point range from cool (blue) to hot (red) as the frequency increases.

Hirshfeld surface with particular values of d_e (distance to the nearest external atomic nucleus) and d_i (distance to the nearest internal atomic nucleus). Colors at each point on the plot range from cool (blue) to hot (red) as the frequency increases. Two long spikes in Figure 4 denote the presence of important intermolecular C–H \cdots O interactions, and the reddish area near $d_i \approx d_e \approx 1.9$ Å reflects the significant contribution made by π -stacking, although the distances are relatively long. In addition, the absence of points near $d_i \approx d_e \approx 1.2$ Å confirms that H \cdots H interactions are of minor importance; similarly, the lack of points near $(d_i, d_e) \approx (1.7, 1.1)$ or $(d_i, d_e) \approx (1.1, 1.7)$ demonstrates that C–H $\cdots\pi$ interactions are not significant. Together, the Hirshfeld surface and fingerprint plot suggest that the conical topology of phosphangulene allows molecules to be stacked with a degree of efficiency, despite low mutual affinity arising from any specific interactions other than dipolar alignment.

As noted by Yamamura and Nabeshima,⁷ converting phosphangulene into the corresponding oxide, sulfide, and selenide (2a–c) makes the cone angle slightly less acute, possibly as a result of decreases in the s -character of the orbital of phosphorus involved in the P -chalcogenide bonds. In addition, forming the chalcogenides adds only one atom to phosphangulene but changes the topology markedly, creating awkwardly shaped molecules that are no longer predisposed to stack. These intriguing early observations suggested to us that further analysis of phosphangulene, its chalcogenides, and related compounds offered a unique opportunity to explore what we have called the “dark side of crystal engineering,” which focuses on what happens when normal patterns of crystallization are thwarted.^{8–11} This approach has begun to yield materials with unusual properties, as well as deeper understanding of subtle factors controlling molecular organization. Previous studies of chalcogenides 2a–c and analogues

Scheme 1

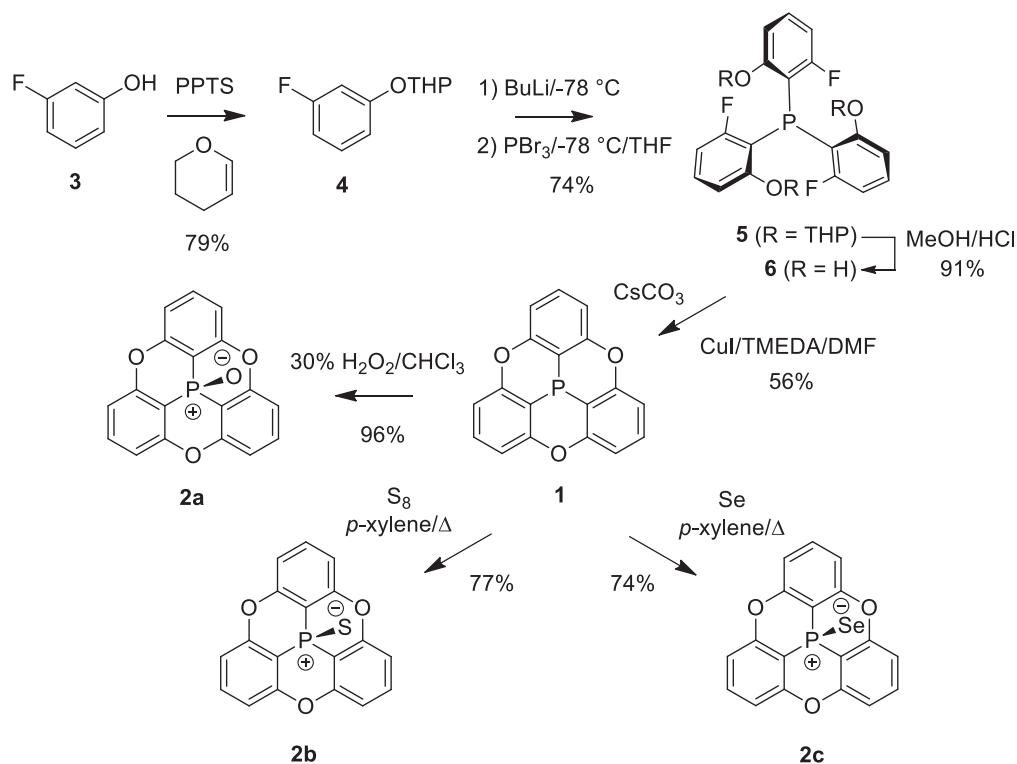


Table 1. Crystallographic Data for Polymorphs A, B, C, D, and E of Phosphangulene Oxide (2a)

polymorph	A ^a	B	C	D	E
crystallization medium	EtOAc	EtOH	EtOH	EtOH	EtOH
formula	C ₁₈ H ₉ O ₄ P				
crystal system	monoclinic	monoclinic	orthorhombic	orthorhombic	monoclinic
space group	P2 ₁ /n	P2 ₁ /c	Pbca	Pca2 ₁	P2 ₁
a (Å)	10.0356(15)	28.5547(11)	12.0850(6)	11.6101(3)	9.9199(5)
b (Å)	25.043(4)	16.6794(6)	7.4412(4)	16.6814(5)	11.8932(5)
c (Å)	10.6453(16)	11.6200(4)	29.7220(16)	28.2286(8)	11.8950(6)
α (deg)	90	90	90	90	90
β (deg)	94.420(1)	98.990(1)	90	90	101.879(3)
γ (deg)	90	90	90	90	90
V (Å ³)	2667.4(7)	5466.3(3)	2672.8(2)	5467.1(3)	1373.31(11)
Z	8	16	8	16	4
Z'	2	4	1	4	2
F(000)	1312	2624	1312	2624	656
T (K)	120	150	150	150	150
ρ _{calc} (g cm ⁻³)	1.595	1.556	1.592	1.556	1.549
λ (Å)	0.71073	1.34139	1.34139	1.34139	1.34139
μ (mm ⁻¹)	0.226	1.282	1.307	1.279	1.272
measured reflections	30172	131053	21867	64961	25072
independent reflections	6042	12534	3063	11716	6277
R _{int}	0.0229	0.0351	0.0512	0.0399	0.0362
R _σ	0.0145	0.0133	0.0325	0.0294	0.0299
observed reflections	5812	12089	2650	10862	5983
R ₁ , I > 2σ(I)	0.0332	0.0417	0.0491	0.0475	0.0420
R ₁ , all data	0.0343	0.0426	0.0561	0.0519	0.0447
wR ₂ , I > 2σ(I)	0.0889	0.1078	0.1238	0.1217	0.1068
wR ₂ , all data	0.0904	0.1090	0.1310	0.1266	0.1099
GOF	1.033	1.055	1.088	1.026	1.025
max/min (e Å ⁻³)	0.434/-0.352	0.428/-0.497	0.563/-0.51	0.590/-0.391	1.190/-0.274
Flack parameter	N/A	N/A	N/A	0.006(17)	0.08(3)

^aData taken from the work of Krebs, Yamamura, and co-workers.^{7,13}

confirmed the intuitive expectation that their awkward shape prevents stacking, but other important questions have not been answered, such as what new patterns of organization emerge as alternatives to stacking or what the observed structures reveal about molecular crystallization in general. We have now found that analysis of structural options available to phosphangulene, its chalcogenides, and related compounds sheds light on enduring mysteries, including the origin of high levels of polymorphism, unusually large numbers of molecules in unit cells, and pronounced tendencies to form solvates, solid solutions, and cocrystals.

RESULTS AND DISCUSSION

Syntheses of Phosphangulene and its Chalcogenides. Phosphangulene was synthesized by a modification of the method reported by Krebs and co-workers (Scheme 1).¹ Protection of 3-fluorophenol (3) as its tetrahydropyranyl (THP) ether (4) was achieved efficiently in neat dihydropyran with pyridinium *p*-toluenesulfonate (PPTS) as the acidic catalyst. Metalation of THP ether 4 and subsequent reaction with PBr_3 afforded triarylphosphine 5, as described by Krebs and co-workers,¹ and the protective group was then removed by acid-catalyzed methanolysis to give phosphine 6. Krebs and co-workers reported preparing phosphangulene in 86% yield by heating intermediate 6 with $\text{KO-}t\text{-Bu}$ in *N*-methylpyrrolidinone at 200 °C, but we obtained lower yields despite various attempts to use the reported method. Instead, we turned to an intramolecular Ullmann-type coupling of the type described by Zhang and co-workers.¹² Treatment of intermediate 6 with Cs_2CO_3 and CuI in DMF gave phosphangulene conveniently and reproducibly in 56% yield. Further experiments showed that CuI was necessary and that its use with other bases such as $\text{KO-}t\text{-Bu}$ or K_2CO_3 gave lower yields. Chalcogenides 2a–c were obtained in high yields from phosphangulene by modifications of published methods (Scheme 1).¹⁷ Specifically, oxide 2a was prepared by treatment with 30% aqueous hydrogen peroxide, sulfide 2b by heating with elemental sulfur in xylene, and selenide 2c by an analogous reaction with elemental selenium.

Polymorphs of Phosphangulene Oxide. The characteristic stacking of molecules of phosphangulene cannot be maintained in crystals of chalcogenides 2a–c. The added *P*-chalcogen bonds alter the dipole moment of phosphangulene and create awkward molecular shapes that retain C_{3v} molecular symmetry but can no longer form efficiently packed conical stacks. Confirmation is provided by the earlier work of Krebs, Yamamura, and their co-workers, who reported the structure of crystals of phosphangulene oxide (2a) grown from ethyl acetate (polymorph A).^{7,13} More thorough analysis has revealed four new polymorphs B–E. The new polymorphs are described below, after a summary of the structure of known polymorph A to allow comparison.

Polymorph A of Oxide 2a. Crystals grown from ethyl acetate belong to the monoclinic space group $P2_1/n$, with $Z = 8$ and $Z' = 2$. The same structure is also produced by crystallization from anhydrous ethanol. Other crystallographic data are summarized in Table 1, and views of the structure are presented in Figures 5, 6, and 7. Conical stacking is not observed; instead, the structure consists of pairs of symmetry-inequivalent molecules of oxide 2a (Figure 5), held in an offset clamshell arrangement by multiple $\text{C-H}\cdots\pi$ interactions despite a locally unfavorable orientation of molecular dipoles. Adjacent pairs form $\text{C-H}\cdots\text{O}$ interactions involving atoms of

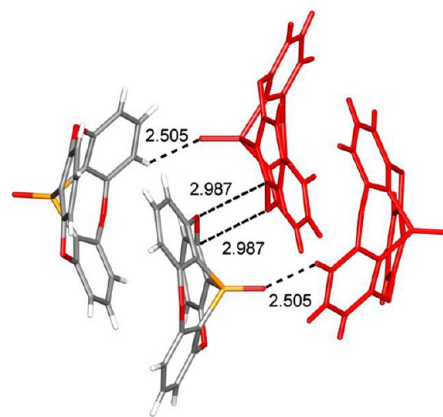


Figure 5. Representation of the structure of crystals of phosphangulene oxide (2a) grown from ethyl acetate (polymorph A). Two molecules that interact to form an offset clamshell pair are highlighted in red, and a second pair is shown with atoms in normal colors. Selected $\text{C-H}\cdots\text{O}$ interactions and $\text{C}\cdots\text{O}$ contacts are marked by broken lines, with distances given in Å.

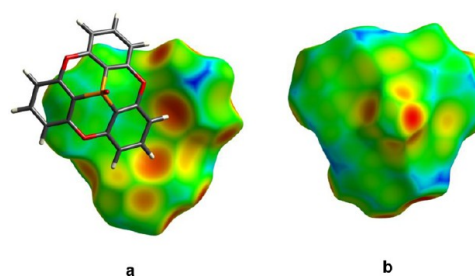


Figure 6. (a) Hirshfeld surface colored by d_e , showing an offset clamshell pair formed by two molecules of oxide 2a in polymorph A. (b) Corresponding surface of one of the convex faces of the pair.

oxygen bonded to phosphorus (2.505 Å in the illustrated pairs), as well as unusually short $\text{C}\cdots\text{O}$ contacts (2.987 Å) involving atoms of oxygen in the phosphangulene rings.

Key features of the structure are highlighted by the Hirshfeld surfaces shown in Figure 6. In particular, conspicuous red spots on the concave surface (Figure 6a) arise from multiple $\text{C-H}\cdots\pi$ interactions, and red spots near the center of the convex surface reflect the formation of $\text{C-H}\cdots\text{O}$ interactions involving atoms of oxygen bonded to phosphorus (Figure 6b). The striking dissimilarity of the structures of phosphangulene and oxide 2a is underscored by the fingerprint plots in Figure 7. The two symmetry-inequivalent molecules in the asymmetric unit of polymorph A engage in closely similar interactions, as demonstrated by the overall resemblance of Figures 7a and 7b. Features of particular interest that distinguish the plots from that of phosphangulene (Figure 4) are (1) numerous $\text{H}\cdots\text{H}$ interactions, as indicated by the density of points near $d_i \approx d_e \approx 1.1$ Å, (2) significant wings near $(d_i, d_e) \approx (1.8, 1.1)$ and $(d_i, d_e) \approx (1.1, 1.8)$, which correspond to $\text{C-H}\cdots\pi$ interactions, and (3) the many large values of d_i and d_e observed in Figure 7, which extend to approximately 2.7 Å. In sharp contrast, the plot corresponding to phosphangulene is compact and bounded by $d_i \approx d_e \approx 2.3$ Å (Figure 4).

Together, the Hirshfeld surfaces and fingerprint plots suggest that oxide 2a has no compelling reason to crystallize in any particular way, despite its relatively rigid and symmetric molecular structure. Instead, crystallization is forced to produce a structure with many suboptimal interactions, and

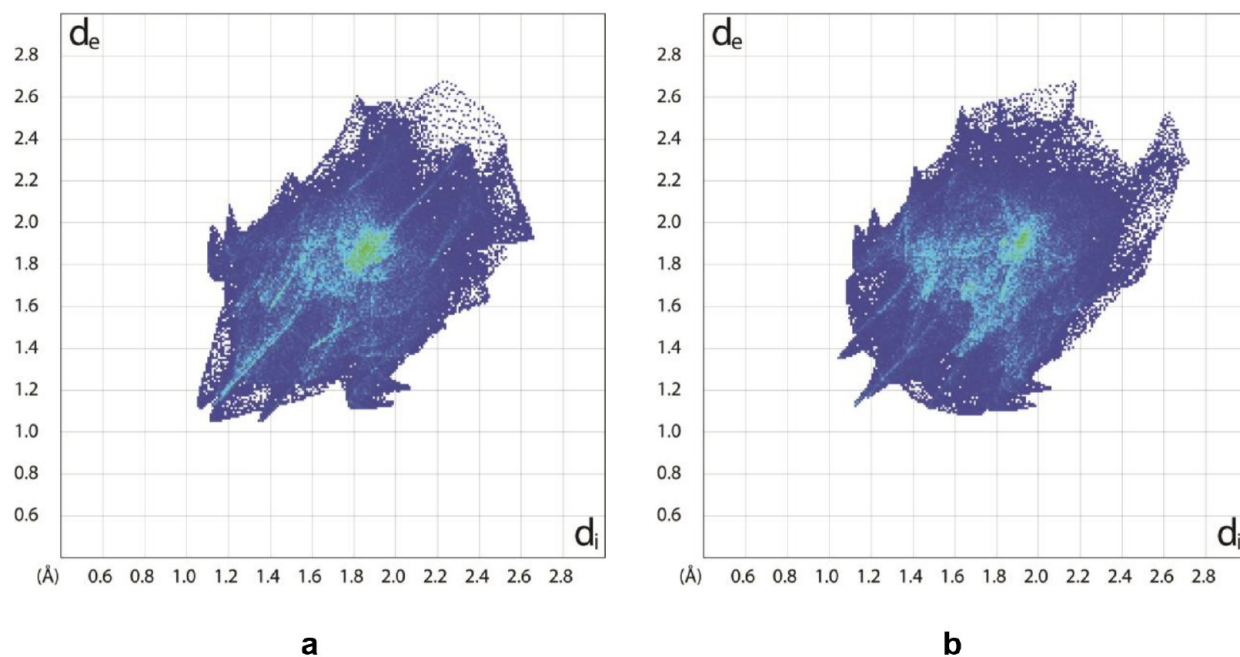


Figure 7. Fingerprint plots of Hirshfeld surfaces for the two symmetry-inequivalent molecules of oxide **2a** in polymorph A.

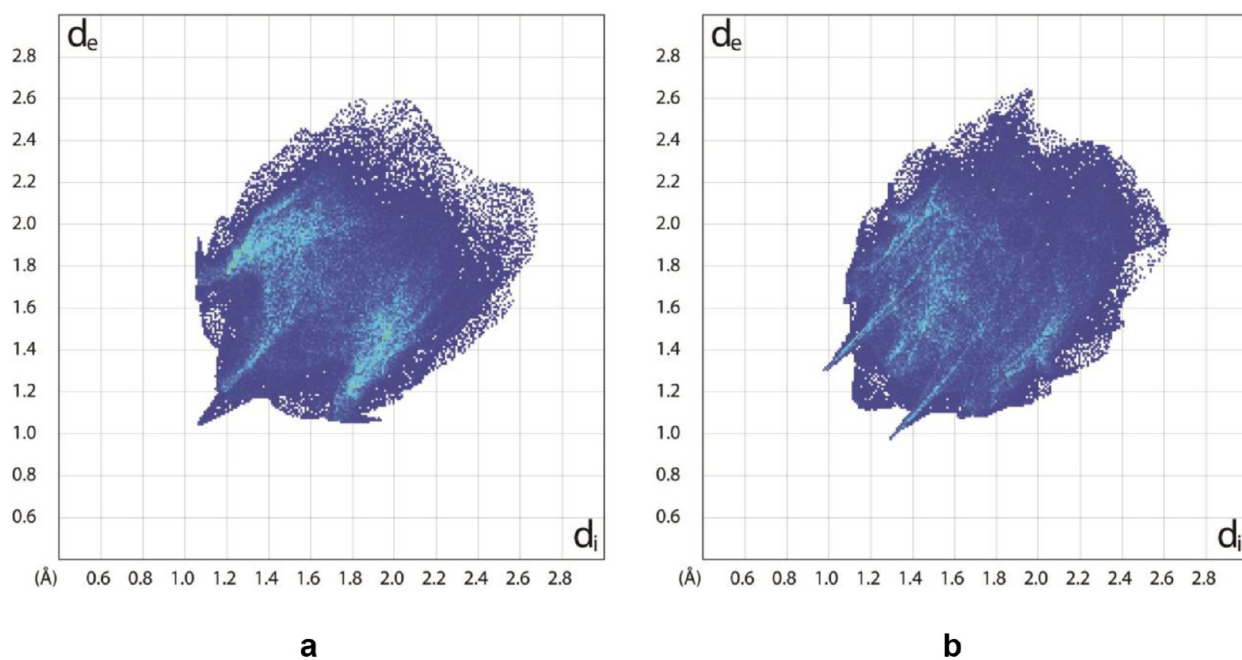


Figure 8. (a) Representative fingerprint plot of the Hirshfeld surface of one of the four symmetry-inequivalent molecules of triphenylphosphine in the triclinic *P1* polymorph. (b) Fingerprint plot of the Hirshfeld surface of a molecule of triphenylphosphine oxide in the orthorhombic *PbcA* form.

multiple molecules are used to create a unit cell with acceptable packing. The high frequency of large intermolecular separations in the fingerprint plots of Figure 7, as indicated by the density of points with coordinates exceeding 2.3 Å, reveals that the behavior of oxide **2a** resembles that of classic clathrate-forming compounds such as hydroquinone and Dianin's compound. Both enclose suitable guests but can also form guest-free *R*-3 crystals with significant unoccupied volume.^{14,15} Fingerprint plots of the Hirshfeld surfaces of molecules in such structures are strikingly extended.

The markedly different packing of phosphangulene and its oxide can also be underscored by comparing voids in their

structures, as assessed by using spheres of variable radius to probe accessible volumes lying between the van der Waals surfaces of the constituent molecules. For crystals of phosphangulene and polymorph A of oxide **2a**, the Kitaigorodsky packing coefficients are similar (0.689 and 0.705, respectively, at 293 K), but the structure of oxide **2a** incorporates much larger voids. For example, a probe sphere of radius 0.8 Å can occupy 6% of the volume of crystals of polymorph A but cannot be accommodated anywhere within the structure of phosphangulene. Adding an atom of oxygen to phosphangulene interferes substantially with molecular packing, as expected, whereas such changes do not result routinely

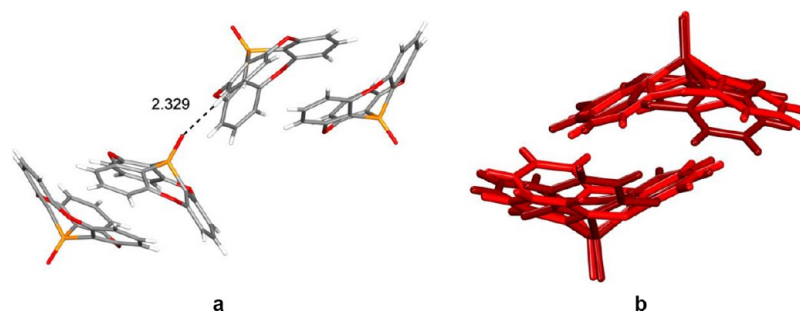


Figure 9. (a) Representation of the structure of needle-shaped crystals of oxide **2a** grown from anhydrous ethanol (polymorph B). Two adjacent inequivalent clamshell pairs are shown with atoms in normal colors. The shortest C–H···O interaction between pairs is marked by a broken line, with the distance given in Å. (b) Superposition of representative clamshell pairs in the structures of polymorphs A and B, with different pairs shown in shades of red.

when triarylphosphines are converted into the corresponding oxides. For example, the structures of the triclinic *P1* polymorph of triphenylphosphine¹⁶ and the orthorhombic *Pbca* form of its oxide¹⁷ are related, as confirmed by comparing the fingerprint plots in Figure 8, which are bounded by similar values of d_i and d_e .

Polymorph B of Oxide 2a. We observed that crystallizing phosphangulene oxide from anhydrous ethanol yielded crystals with different morphologies. Blocks proved to correspond to known polymorph A, whereas needles were shown to be new polymorph B, which crystallized in the monoclinic space group *P2₁/c* with $Z = 16$ and $Z' = 4$. Additional crystallographic data are provided in Table 1, and representations of the structure are shown in Figures 9–10. Again, oxide **2a** forms offset

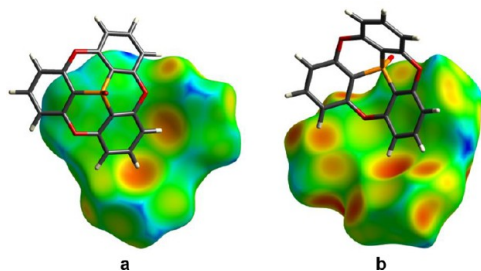


Figure 10. (a) Hirshfeld surface colored by d_e , showing a representative offset clamshell pair of molecules of oxide **2a** in polymorph B. (b) Corresponding surface of adjacent molecules of oxide **2a** in a slipped stack in polymorph C.

clamshell pairs like those observed in polymorph A (Figure 9a). The resemblance of the pairs in the two polymorphs can be highlighted by superimposition (Figure 9b) and by comparison of the Hirshfeld surfaces (Figures 6a and 10a). Conspicuous red spots on the concave surface of molecules in polymorph B reflect C–H··· π interactions that help hold the pairs together, and the structure is also maintained by π -stacking, dipolar alignment, and various C–H···O interactions, including those with H···O distances as short as 2.329 Å (C–H···O–P) and 2.426 Å (C–H···O–C). Portraying structural details is complicated by the high value of Z' , and the representative view in Figure 9a highlights only the shortest C–H···O–P distance between adjacent inequivalent clamshell pairs of oxide **2a**.

All four inequivalent molecules of oxide **2a** in the asymmetric unit of polymorph B have very similar environments, and the single fingerprint plot in Figure 11a is

representative.¹⁸ Moreover, the plot closely resembles those of molecules of oxide **2a** in polymorph A (Figure 7). In both polymorphs A and B, molecules of oxide **2a** produce similar fingerprints arising from H···H interactions (area near $d_i \approx d_e \approx 1.0$ – 1.2 Å), C–H··· π interactions (small wings near $(d_i, d_e) \approx (1.8, 1.1)$ and $(d_i, d_e) \approx (1.1, 1.8)$), and distant π -stacking (light blue area centered on $d_i \approx d_e \approx 1.8$ Å). Of special note is the highly extended nature of all plots, which reach out to $d_i \approx d_e \approx 2.7$ Å. This supports the notion that the molecular structure of oxide **2a** prevents efficient stacking and forces crystallization to occur in various alternative ways, none particularly favorable.

Polymorph C of Oxide 2a. Further evidence for this idea is provided by the existence of polymorph C, which is produced concomitantly with polymorphs A and B during crystallization from anhydrous ethanol.¹⁹ Crystals of polymorph C proved to belong to the orthorhombic space group *Pbca* with $Z = 8$ and $Z' = 1$. Table 1 summarizes additional crystallographic data, and Figure 12 provides a view of the structure, which can be considered to consist of slipped stacks of molecules of oxide **2a** with their dipoles aligned approximately along the *b*-axis. Each stack is surrounded by six others, which are oriented so that there is no net dipole along the *b*-axis.

The Hirshfeld surface (Figure 10b) shows two adjacent molecules in a slipped stack and demonstrates the presence of multiple C–H··· π interactions. The close similarity of the fingerprint plot (Figure 11b) to those of molecules in polymorphs A and B confirms the notion that oxide **2a** cannot be packed efficiently in ways that create optimal interactions. In particular, H···H and C–H··· π distances are long, and π -stacking is weak, as shown by reddish areas in the fingerprint plot near $d_i \approx d_e \approx 1.8$ Å. In addition, the plot is notably extended and reveals a high frequency of coordinates with large values of d_i or d_e ranging up to 2.8 Å. The inability of oxide **2a** to crystallize in ways that allow its constituent atoms to engage in normal intermolecular interactions leads to the formation of multiple unappealing polymorphs with nearly equal stabilities, as demonstrated by the concomitant crystallization of forms A, B, and C.

Polymorph D of Oxide 2a. Additional polymorph D was produced when oxide **2a** was crystallized from anhydrous ethanol or from thiophene. Crystals of polymorph D were found to belong to the orthorhombic space group *Pca2₁* with $Z = 16$ and $Z' = 4$. Other crystallographic data are summarized in Table 1, and representations of the structure are provided in Figures 13a and 14a. Again, the structure consists of offset

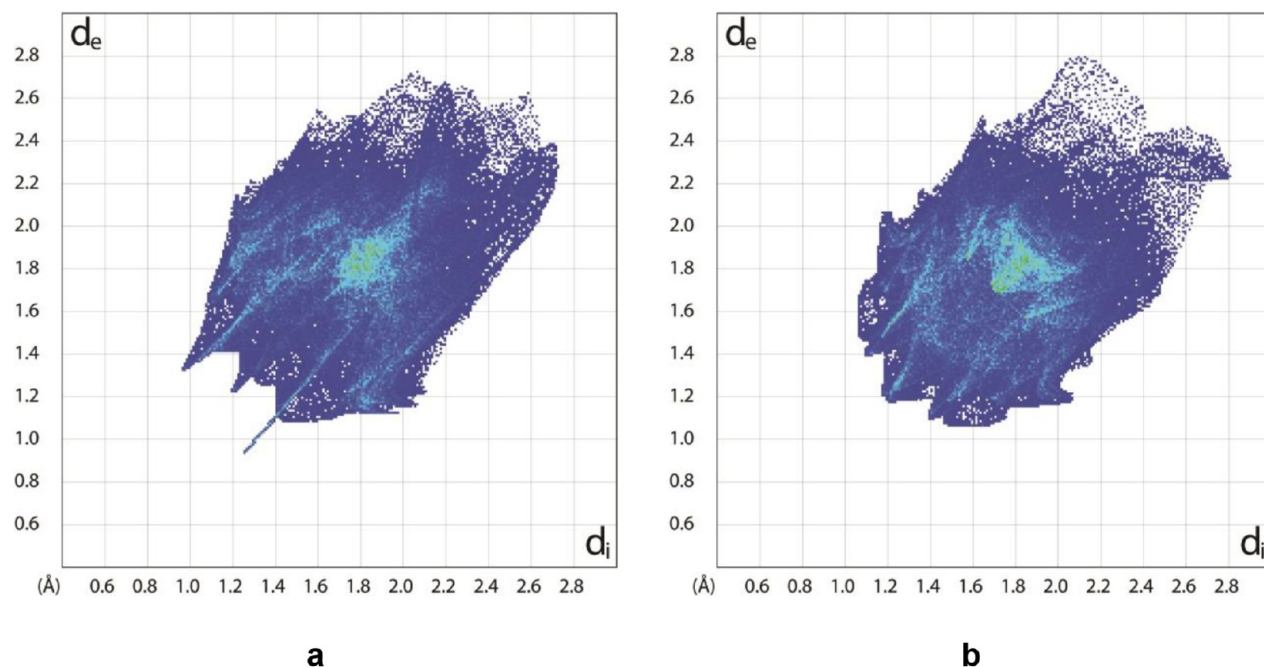


Figure 11. (a) Representative fingerprint plot of the Hirshfeld surface corresponding to one of the four symmetry-inequivalent molecules of oxide 2a in polymorph B. (b) Fingerprint plot for molecules of oxide 2a in polymorph C.

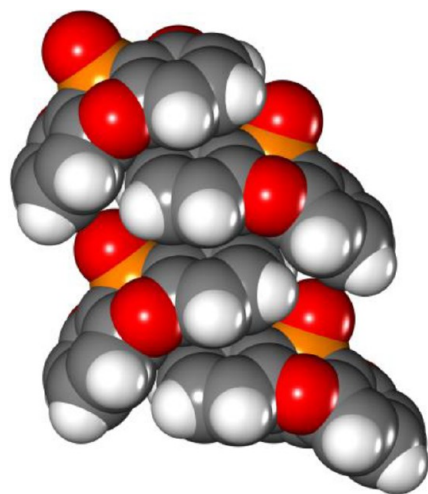


Figure 12. Space-filling representation of part of a slipped stack observed in the structure of polymorph C of oxide 2a. Atoms are shown in normal colors.

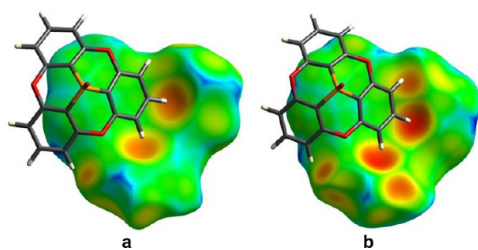


Figure 13. (a) Hirshfeld surface colored by d_e , showing a representative offset clamshell pair formed by two molecules of oxide 2a in polymorph D. (b) Corresponding surface of an offset clamshell pair in polymorph E of oxide 2a.

clamshell pairs similar to those observed in polymorphs A and B (Figure 13a), and fingerprint plots reveal a high frequency of large intermolecular distances (Figure 14a).

Polymorph E of Oxide 2a. A fifth form (polymorph E) resulted when oxide 2a was crystallized from anhydrous ethanol or from CS_2 . Crystals of polymorph E proved to belong to the monoclinic space group $P2_1$ with $Z = 4$ and $Z' = 2$. Table 1 includes additional crystallographic data, and Figures 13b and 14b provide representations of the structure, which show the presence of offset clamshell pairs like those present in polymorphs A, B, and D (Figure 13b), as well as a similarly high frequency of abnormally long intermolecular separations (Figure 14b).

No polymorph of oxide 2a adopts efficient conical stacking of the type observed in crystals of phosphangulene 1 itself. This underscores the disruptive effect of introducing a well-placed atom of oxygen. Adding oxygen also alters the dipole moment and gives rise to new $\text{C}-\text{H}\cdots\text{O}-\text{P}$ interactions in all five polymorphs. The repeated observation of high values of Z' and Z (8, 16, 8, 16, and 4 in polymorphs A, B, C, D, and E, respectively) reinforces the hypothesis that the inherently awkward shape of oxide 2a prevents crystallization from yielding structures in which the constituent atoms have normal intermolecular interactions. This favors the formation of multiple polymorphs that are similar in energy and must use multiple inequivalent molecules to ensure satisfactory packing.^{20–22} In essence, oxide 2a is condemned to crystallize in ways that reflect unsatisfactory compromises: in particular, the conical aromatic surface cannot be packed efficiently in the manner of phosphangulene, nor can it engage fully in $\text{H}\cdots\text{H}$, $\text{C}-\text{H}\cdots\pi$, and $\pi\cdots\pi$ interactions of the type that stabilize stacks and herringbone arrangements of planar aromatic analogues.

As shown in Figure 15, various intermolecular interactions make similar contributions to the Hirshfeld surfaces of all of the polymorphs of oxide 2a, whereas the contributions differ widely from those observed in the structure of phosphangulene

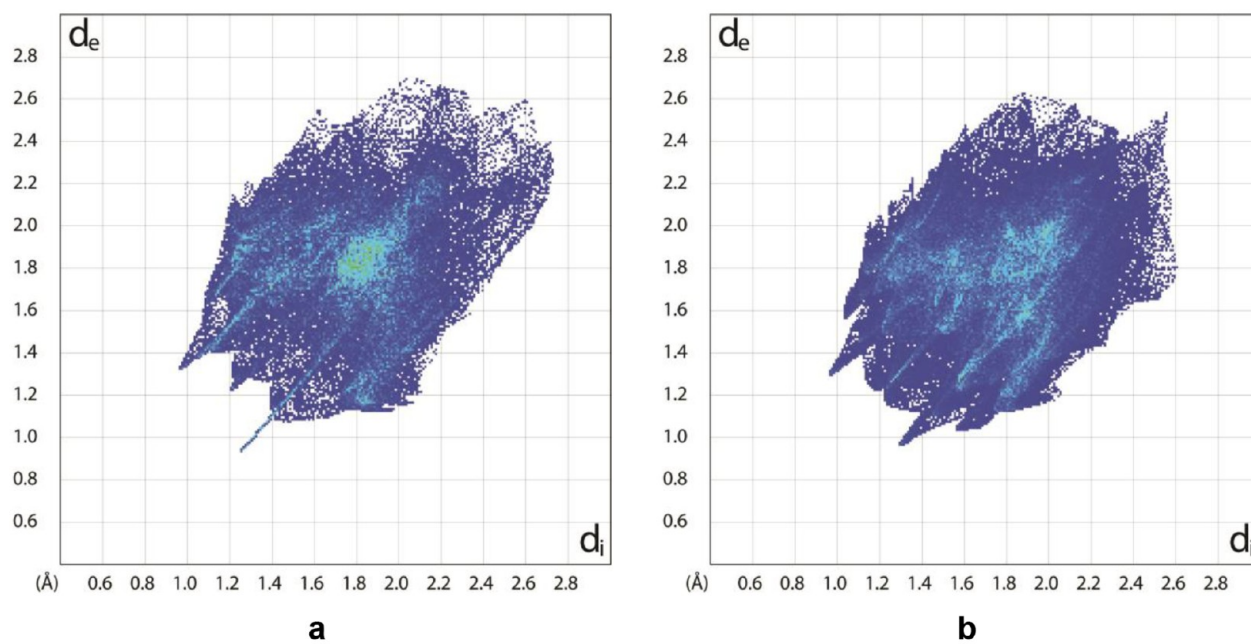


Figure 14. (a) Representative fingerprint plot of the Hirshfeld surface for one of the four symmetry-inequivalent molecules of oxide **2a** in polymorph D. (b) Fingerprint plot for molecules of oxide **2a** in polymorph E.

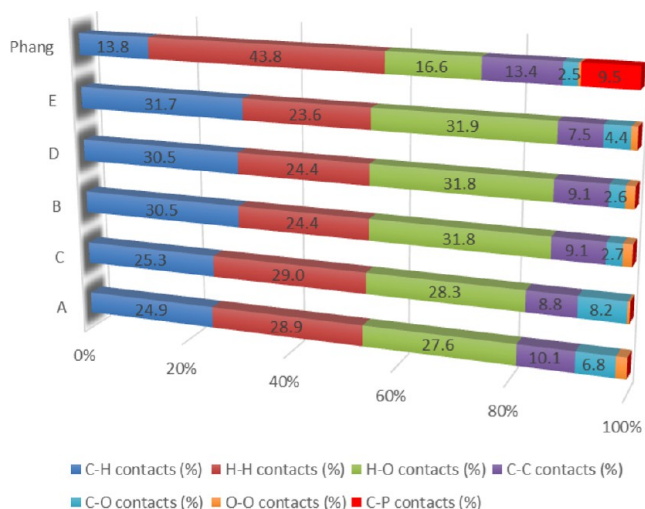


Figure 15. Percentage contributions made by various intermolecular interactions to the Hirshfeld surfaces of representative molecules in the structures of phosphangulene and oxide **2a** (polymorphs A–E). Phosphangulene is shown as Phang, and polymorphs A–E appear in order of the importance of C–H interactions.

1. The crystallographic parameters in Table 1, along with other observations such as the formation of all five polymorphs A–E during crystallization from anhydrous ethanol,¹⁹ do not provide definitive evidence for placing the polymorphs in any particular order of thermodynamic stability. However, the low densities, high values of Z , and relatively low Kitaigorodsky packing coefficients (0.704–0.707 at 150 K) found for polymorphs B, D, and E suggest that they are the least stable. Moreover, we observed the transformation of polymorph B into polymorphs A and C during extended exposure to anhydrous ethanol. Concomitant crystallizations and polymorphic interconversions prevented us from obtaining pure samples for more detailed analysis by differential scanning calorimetry. In principle, computational approaches can be

used to estimate lattice energies and to compare the stabilities of polymorphs; however, current methods cannot be expected to provide reliable guidance in the case of forms A–E of oxide **2a**, which have high values of Z/Z' and closely similar energies, as demonstrated by their coexistence under equilibrating conditions.²³

Only one polymorph of phosphangulene has been reported, and earlier workers noted a single form of oxide **2a**. In this context, we were surprised to observe four new polymorphs, without making any systematic effort to find others. Oxide **2a** is less highly polymorphic than the intensively studied compound 5-methyl-2-[(2-nitrophenyl)amino]-3-thiophene-carbonitrile (ROY), which exists in 10 fully characterized forms and remains one of the most highly polymorphic substances in the Cambridge Structural Database (CSD).^{24–27} Unlike ROY, however, oxide **2a** is a hexacyclic molecule with a well-defined shape, so its rich polymorphic diversity does not arise from an ability to adopt multiple conformations. The CSD now includes more than one million entries, but recent analyses have identified only 13 compounds that are known to exist in more than four fully characterized polymorphic forms.²⁶ Nearly all of these special molecules are flexible and crystallize as different conformers. Oxide **2a** is among the rare examples that are both highly polymorphic and virtually inflexible. As a result, oxide **2a** and its analogues allow the origin of polymorphism to be probed in the absence of other contributing factors. Our observations suggest that the awkward topology of these compounds makes efficient stacking impossible and forces crystallization to occur in ways that lead to many suboptimal intermolecular contacts, thereby expanding the scope for producing polymorphic forms with similar energies. It is also possible that the conical topology and polarity of oxide **2a** inhibit displacements and reorientations needed to convert metastable arrangements into forms of lower energy.

Previous statistical analyses of the CSD have led to assertions that molecular flexibility and the incidence of

Table 2. Crystallographic Data for Polymorphs A and B of Phosphangulene Sulfide (2b) and for Polymorphs A, B, and C of Phosphangulene Selenide (2c)

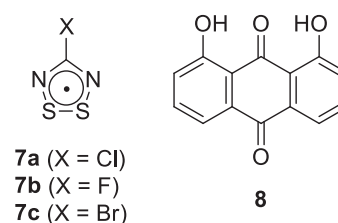
compound	sulfide 2b polymorph A ^a	sulfide 2b polymorph B	selenide 2c polymorph A ^a	selenide 2c polymorph B	selenide 2c polymorph C
crystallization medium	CH ₂ Cl ₂ /hexane	EtOH	CHCl ₃ /hexane	CS ₂	CS ₂
crystal system	monoclinic	orthorhombic	orthorhombic	monoclinic	monoclinic
space group	<i>P</i> ₂ ₁ / <i>c</i>	<i>Pbca</i>	<i>Pbca</i>	<i>P</i> ₂ ₁ / <i>c</i>	<i>I</i> ₂ / <i>a</i>
<i>a</i> (Å)	15.112(5)	14.7446(3)	12.9896(19)	15.0217(6)	14.1307(8)
<i>b</i> (Å)	13.276(4)	13.0971(3)	15.120(2)	13.5252(5)	6.9551(4)
<i>c</i> (Å)	14.291(5)	14.9443(3)	14.872(2)	14.4528(5)	29.079(2)
α (deg)	90	90	90	90	90
β (deg)	93.096(3)	90	90	93.393(2)	90.359(2)
γ (deg)	90	90	90	90	90
<i>V</i> (Å ³)	2863.1(16)	2885.92(11)	2920.8(8)	2931.25(19)	2857.9(3)
<i>Z</i>	8	8	8	8	8
<i>Z'</i>	2	1	1	2	1
<i>F</i> (000)	1376	1376	1520	1520	1520
<i>T</i> (K)	120	105	120	150	150
ρ_{calc} (g cm ⁻³)	1.560	1.548	1.743	1.737	1.781
λ (Å)	0.71073	1.34139	0.71073	1.34139	1.34139
μ (mm ⁻¹)	0.350	2.049	2.692	3.046	3.124
measured reflections	32254	30130	15435	78953	52256
independent reflections	6592	3574	3339	6425	3240
<i>R</i> _{int}	0.0425	0.0274	0.0301	0.0536	0.0464
<i>R</i> _{σ}	0.0345	0.0154	0.0216	0.0232	0.0183
observed reflections	5294	3406	2877	5234	3158
<i>R</i> ₁ , <i>I</i> > 2 σ (<i>I</i>)	0.0336	0.0294	0.0512	0.0320	0.0632
<i>R</i> ₁ , all data	0.0521	0.0306	0.0563	0.0456	0.0647
<i>wR</i> ₂ , <i>I</i> > 2 σ (<i>I</i>)	0.0863	0.0847	0.1339	0.0745	0.1756
<i>wR</i> ₂ , all data	0.0934	0.0857	0.1409	0.0825	0.1775
GOF	1.034	1.051	1.059	1.056	1.054
max/min (e Å ⁻³)	0.474/−0.348	0.456/−0.222	2.369/−0.494	0.397/−0.564	3.205/−1.56

^aData taken from the work of Yamamura and Nabeshima.⁷

polymorphism are not correlated.^{28–30} Nevertheless, the quest to identify general structural features favoring polymorphism and high values of *Z/Z'* remains an active area of study. If predisposing features exist and can be identified, their discovery would have a significant practical impact by expanding the range of different ordered materials that can be derived from a single molecular entity. However, the notion that compounds with multiple polymorphic forms or high values of *Z/Z'* are exceptional and may have underlying shared features is not universally accepted. Dissenting opinions include those of McCrone, who famously stated “. . . that every compound has different polymorphic forms and that, in general, the number of forms known for a given compound is proportional to the time and energy spent in research on that compound.”³¹ In addition, Gavezzotti has suggested that each case of elevated values of *Z'* “. . . may be a story in itself.”³²

Much of what is believed to be true about high levels of polymorphism and large values of *Z/Z'* reflects purely statistical analyses of the CSD or smaller sets of data, often related to drugs and intermediates used in their synthesis, which do not represent the full scope of molecular diversity. In contrast, surprisingly little effort has been devoted to close comparative scrutiny of the structures of highly polymorphic substances or to experimental studies of compounds specifically devised to test conjectures about the origins of polymorphism and high values of *Z/Z'*. Of the 13 compounds recently highlighted because they are known to exist in more than four polymorphic forms,²⁶ only the 4-chloro-1,2,3,5-dithiadiazolyl radical (7a)^{33,34} and 1,8-dihydroxyanthraqui-

none (8)^{35,36} resemble oxide 2a by existing primarily in a single conformation.



This places compounds 2a, 7a, and 8 in an intriguing subset of elite highly polymorphic compounds and challenges chemists to identify specific structural features that explain their special behavior. The polymorphic diversity of radical 7a presumably arises in part from its strong self-association, which creates isomeric dimers that resemble distinct covalently bonded species and therefore crystallize differently. Notably, however, the behavior of radical 7a does not extend to close analogues such as fluoride 7b and bromide 7c, which have not yielded multiple polymorphs despite efforts to make them.³³ As a result, the example of radical 7a is “a story in itself” that does not tell how to design any other highly polymorphic compounds, even those with a close structural relationship.

1,8-Dihydroxyanthraquinone (8) is a natural product derived from glycosides that have long been used as laxatives. Its high polymorphism has complex origins, including the ability to engage in multiple intermolecular O–H⋯O hydrogen-bonding motifs. However, none of the observed structures exhibits any clear signs of inefficient packing. In particular, the

values of Z' are generally small (1, 2, 4, 1, and 0.5 for the five known polymorphs), and the fingerprint plots are compact, with a low frequency of abnormally long distances to atoms in neighboring molecules (beyond $d_i \approx d_e \approx 2.4$ Å). As in the case of radical **7a**, the behavior of anthraquinone **8** does not point unerringly to any other compounds that would also be expected to be highly polymorphic. The examples of compounds **7a** and **8** thereby provide grounds for the gloomy conjecture that “polymorphism is unpredictable on the basis of molecular structure.”³⁰

Phosphangulene chalcogenides **2a–c** have let us put this notion to a stringent experimental test. The special features that appear to induce oxide **2a** to form multiple polymorphs with high values of Z/Z' remain essentially unchanged in analogues **2b–c**; in particular, the retained awkward topology is expected to continue to prevent crystallization from occurring in fully satisfactory ways. If polymorphism is in fact unpredictable, however, then sulfide **2b** and selenide **2c** should not necessarily behave like oxide **2a**.

Polymorphs of Phosphangulene Sulfide. Yamamura and Nabeshima previously solved the structure of crystals of sulfide **2b** grown from CH_2Cl_2 /hexane, which will be referred to as polymorph A.⁷ By crystallizing sulfide **2b** from anhydrous ethanol, we obtained new polymorph B. Its structure is described below, after a brief analysis of known polymorph A to allow comparison.

Polymorph A of Sulfide 2b. Crystals of known form A belong to the monoclinic space group $P2_1/c$ with $Z = 8$ and $Z' = 2$. Additional crystallographic data are provided in Table 2, and representative views of the structure are shown in Figures 16 and 17a. Conical stacking is prevented, as expected, and

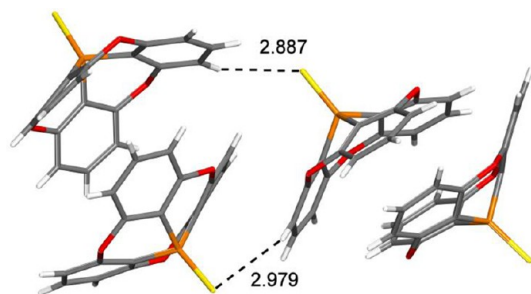


Figure 16. Representation of the structure of crystals of sulfide **2b** (polymorph A). Two adjacent offset clamshell pairs of molecules are illustrated with atoms of carbon in gray, hydrogen in white, oxygen in red, phosphorus in orange, and sulfur in yellow. C–H···S interactions are marked by broken lines, with the distances given in Å.

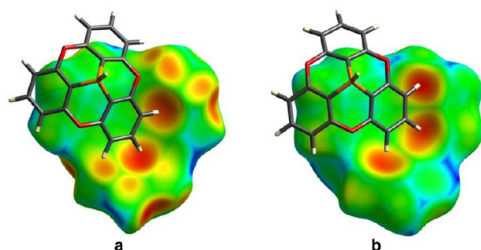


Figure 17. (a) Hirshfeld surface colored by d_e , showing a representative offset clamshell pair formed by two molecules of sulfide **2b** in polymorph A. (b) Corresponding surface of an offset clamshell pair in polymorph B of sulfide **2b**.

molecules form offset clamshell pairs like those present in multiple polymorphs of oxide **2a** (Figure 16). This observation suggests that pairing is a fundamental preference of all phosphangulene chalcogenides, not a phenomenon resulting uniquely from C–H···O–P interactions in oxide **2a**. The Hirshfeld surface of paired molecules of sulfide **2b** (Figure 17a) closely resembles the corresponding surfaces of various polymorphs of oxide **2a** and shows that the pairs are again joined by multiple C–H··· π interactions. The fingerprint plot in Figure 18a demonstrates that the structure of polymorph A of sulfide **2b** is maintained by various interactions, including π -stacking, C–H··· π interactions, C–H···O interactions, and C–H···S interactions. As in the case of polymorphs A–E of oxide **2a**, the fingerprint plot is notably extended and shows a high frequency of coordinates with values of d_i or d_e as large as 2.8 Å. The plot thereby confirms that sulfide **2b**, like oxide **2a**, is forced by topology to pack in ways that poorly exploit the potential of the constituent atoms to engage in stabilizing intermolecular contacts. As a result, small changes in structural parameters can be accommodated without incurring significant energetic penalties, and the range of accessible polymorphs is broadened.

Polymorph B of Sulfide 2b. Crystallization of sulfide **2b** from anhydrous ethanol yielded a new form, polymorph B. The crystals were found to belong to the orthorhombic space group $Pbca$ with $Z = 8$ and $Z' = 1$, and other crystallographic data are summarized in Table 2. The Hirshfeld surface in Figure 17b confirms that polymorph B incorporates offset clamshell pairs joined by multiple C–H··· π interactions, as found in polymorph A of sulfide **2b** and in polymorphs A, B, D, and E of oxide **2a**. Unlike polymorph A of sulfide **2b**, however, polymorph B does not have any C–H···O or C–H···S contacts shorter than the sum of the van der Waals radii. The fingerprint plot (Figure 18b) reveals that intermolecular separations in polymorph B are unusually large; in particular, there are no points on the Hirshfeld surface with values of d_i or d_e less than 1.3 Å. Polymorph A is denser than polymorph B and therefore appears to be more stable.

Polymorphs of Phosphangulene Selenide. With the polymorphism of sulfide **2b** established, we did not search systematically for other forms, but instead examined the crystallization of selenide **2c**. We were confident that the coherent behavior of oxide **2a** and sulfide **2b**, including their polymorphism, formation of crystals with large values of Z/Z' , and abnormally high frequencies of long intermolecular distances, reflected basic principles of molecular design and organization that would also govern the properties of selenide **2c**. In previous work, Yamamura and Nabeshima reported the structure of crystals of selenide **2c** grown from CHCl_3 /hexane, which will be referred to as polymorph A.⁷ We have found that new polymorphs result when selenide **2c** is crystallized under other conditions. Their structures are described below, following an analysis of known polymorph A to allow comparison.

Polymorph A of Selenide 2c. Crystals of selenide **2c** grown from CHCl_3 /hexane belong to the orthorhombic space group $Pbca$ with $Z = 8$ and $Z' = 1$. Table 2 summarizes additional crystallographic data, and Figure 19a provides a representative view of the structure. Polymorph A of selenide **2c** and polymorph B of sulfide **2b** are isostructural. Conical stacking is obstructed, as expected, and molecules of selenide **2c** form offset clamshell pairs like those produced by oxide **2a** and sulfide **2b**. Molecular association in the structure is

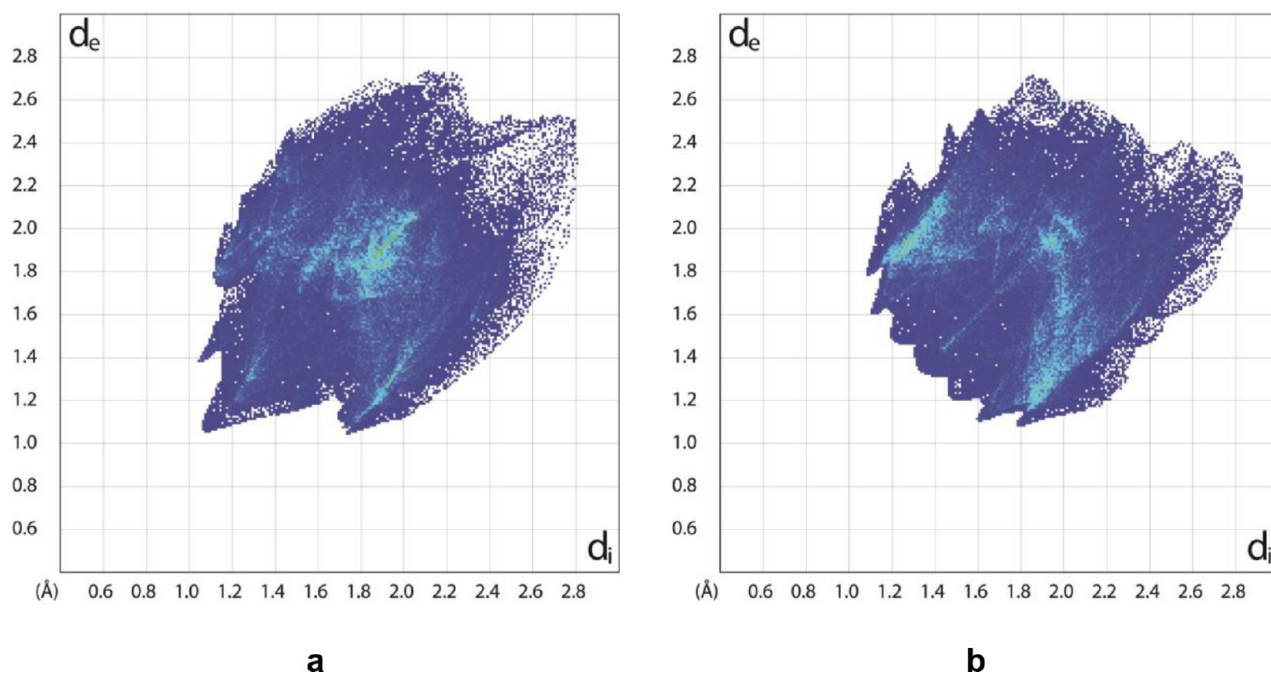


Figure 18. (a) Representative fingerprint plot of the Hirshfeld surface for one of the two symmetry-inequivalent molecules of sulfide **2b** in polymorph A. (b) Fingerprint plot for molecules of sulfide **2b** in polymorph B.

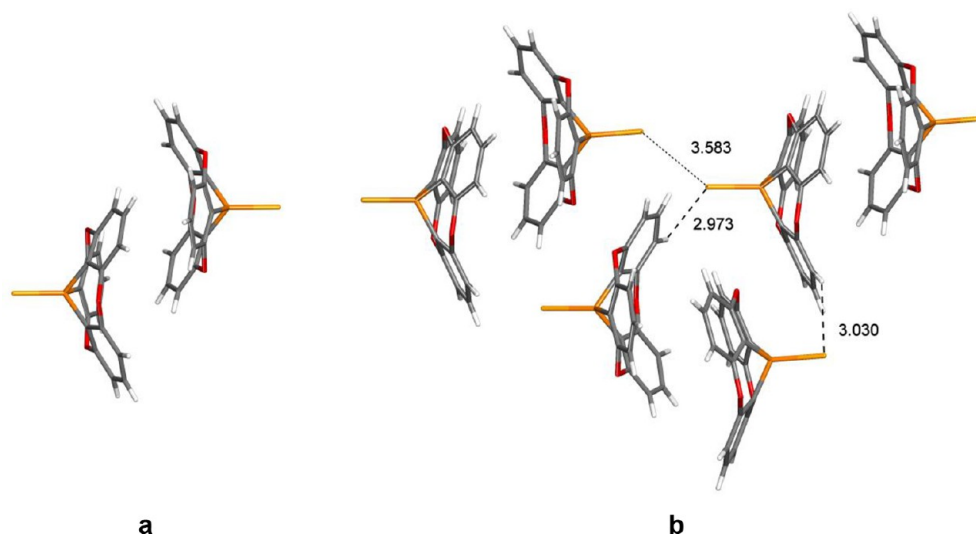


Figure 19. Representations of the structures of crystals of selenide **2c** grown from $\text{CHCl}_3/\text{hexane}$ (polymorph A) and from CS_2 (polymorph B). (a) Offset clamshell pair observed in polymorph A. (b) Three adjacent offset clamshell pairs in polymorph B. Both images show atoms of carbon in gray, hydrogen in white, oxygen in red, phosphorus in orange, and selenium in yellow. Selected C–H...Se and Se...Se interactions are marked by broken lines, with the distances given in Å.

governed primarily by C–H... π and C–H...O interactions, as shown by the Hirshfeld surface of paired molecules in Figure 20a. Again, the fingerprint plot is abnormally extended, with values of d_i or d_e reaching out beyond 2.7 Å.

Polymorph B of Selenide 2c. New polymorphs B and C were obtained concomitantly by crystallizing selenide **2c** from CS_2 . Crystals of form B proved to belong to the monoclinic space group $P2_1/c$ with $Z = 8$ and $Z' = 2$. Table 2 summarizes additional crystallographic data, and Figure 19b shows that the structure is composed of offset clamshell pairs like those formed by polymorph A of selenide **2c** and by various polymorphs of oxide **2a** and sulfide **2b**. Form B of selenide **2c** and form A of sulfide **2b** are isostructural. The Hirshfeld

surface corresponding to form B of selenide **2c** confirms that the pairs are held together by multiple C–H... π interactions (Figure 20b). Other contacts shorter than the sum of the van der Waals radii include C–H...Se interactions (2.973 and 3.030 Å) and Se...Se interactions (3.583 Å), as illustrated in Figure 19b. The fingerprint plot (Figure 21b) is even more extended than that of polymorph A of selenide **2c**, and values of d_i reach 2.9 Å.

Polymorph C of Selenide 2c. Crystals of concomitant polymorph C were found to belong to the monoclinic space group $I2/a$ with $Z = 8$ and $Z' = 1$. Other crystallographic details appear in Table 2, and a view of the structure is provided in Figure 22. The structure is devoid of noteworthy

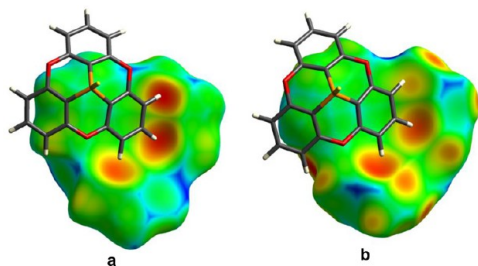


Figure 20. (a) Hirshfeld surface colored by d_e , showing an offset clamshell pair formed by molecules of selenide **2c** in polymorph A. (b) Corresponding surface of a representative offset clamshell pair in polymorph B of selenide **2c**.

interactions, and it can be considered to be composed of adjacent columns in which widely separated molecules (6.955 Å) are stacked with their P–Se bonds aligned approximately with the b -axis. The convex and concave faces of the Hirshfeld surface (Figure 23) indicate that the structure is maintained in part by C–H $\cdots\pi$ interactions between columns, and the corresponding fingerprint plot extends to large values of d_i and d_e (Figure 24).

The inability to form stacks like those favored by phosphangulene forces chalcogenides **2a–c** to accept unattractive alternatives, particularly structures built from offset clamshell pairs held together by multiple C–H $\cdots\pi$ interactions. Figure 25 shows the superimposition of six representative pairs that are present in the structures of oxide **2a** (polymorphs A and B), sulfide **2b** (polymorphs A and B), and selenide **2c** (polymorphs A and B). The figure confirms that a similar association is conserved throughout the series, but the structural details vary substantially. This suggests that chalcogenides **2a–c** are highly polymorphic partly because they can form a multitude of pairs that have slightly differing geometries, closely similar energies, and numerous ways to pack in crystal lattices.

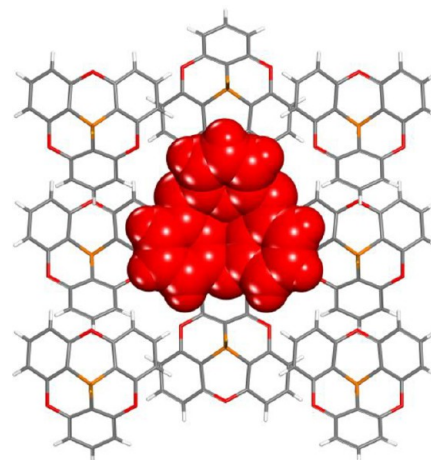


Figure 22. Representation of the structure of crystals of selenide **2c** (polymorph C). View along the b -axis, showing how a central column of widely separated molecules (in red) is surrounded by eight other loose stacks. Unless otherwise indicated, atoms are shown in normal colors.

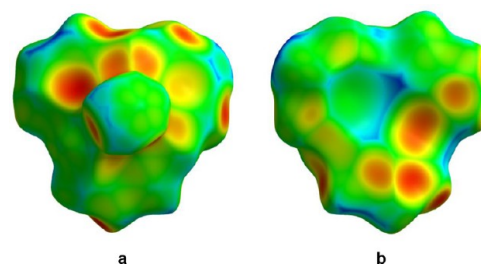


Figure 23. (a) Hirshfeld surface colored by d_e , showing the convex face of a molecule of selenide **2c** in polymorph C. (b) Corresponding concave face.

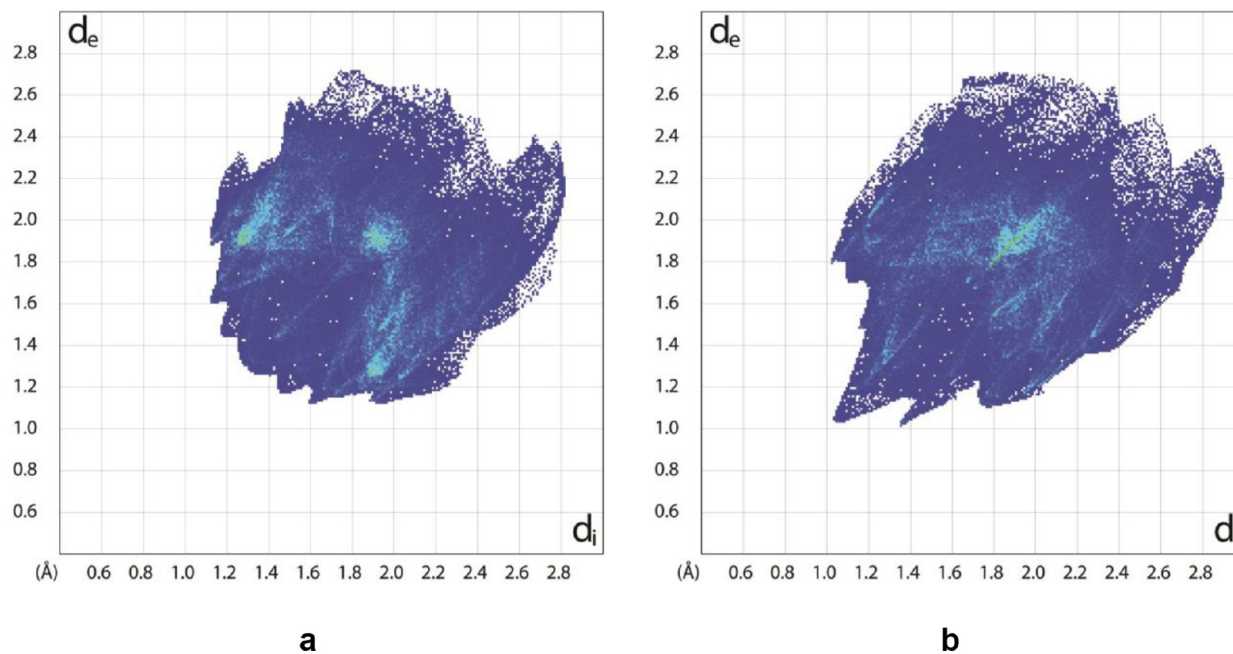


Figure 21. (a) Representative fingerprint plot of the Hirshfeld surface for one of the two symmetry-inequivalent molecules of selenide **2c** in polymorph A. (b) Fingerprint plot for molecules of selenide **2c** in polymorph B.

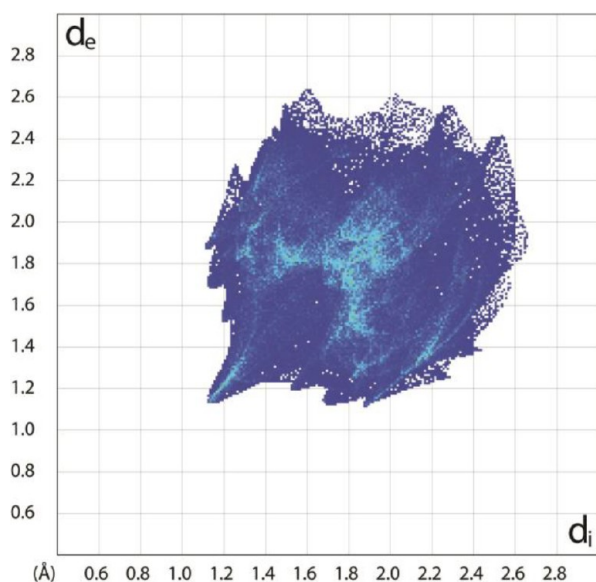


Figure 24. Fingerprint plot for molecules of selenide **2c** in polymorph C.

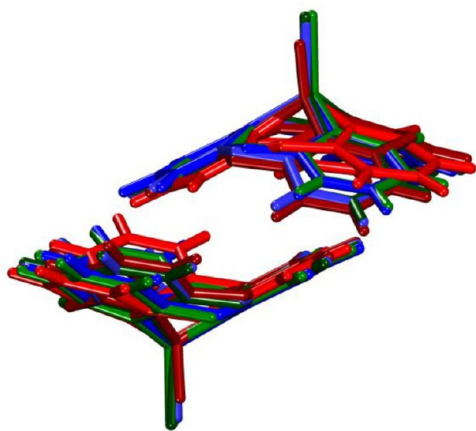


Figure 25. Superimposition of six representative offset clamshell pairs present in the structures of oxide **2a** (polymorphs A and B in red and dark red), sulfide **2b** (polymorphs A and B in blue and dark blue), and selenide **2c** (polymorphs A and B in green and dark green).

Ability of Phosphangulene Chalcogenides 2a–c To Form Crystalline Solid Solutions, Pseudo-Polymorphs, and Cocrystals. The distinctive shape of chalcogenides **2a–c** prevents efficient packing and forces crystallization to occur in ways that are significantly flawed, with high frequencies of long intermolecular contacts. Polymorphism is thereby favored, and multiple molecules are needed to construct unit cells with acceptable packing. We reasoned that if chalcogenides **2a–c** cannot in fact crystallize in fully satisfactory ways, then they should be disposed to form structures that accommodate other molecules.

To test this notion, we crystallized equimolar mixtures of phosphangulene and oxide **2a** from ethyl acetate, and we observed the formation of both needles and blocks. The needles proved to be phosphangulene uncontaminated by oxide **2a**. This indicates that crystallization of phosphangulene by stacking is kinetically favorable, as well as topologically attractive, and that the lattice effectively excludes molecules of oxide **2a**, which are larger and awkwardly shaped. Concurrently

formed block-shaped crystals were found to have the structure of polymorph C of oxide **2a**, but they contained ratios of oxide **2a** and phosphangulene that varied according to the changing composition of the mother liquors. Blocks appearing early in the crystallization were shown to have the 1:1 composition of the initial mother liquors, whereas crystals formed later were progressively enriched in oxide **2a** as pure phosphangulene was gradually removed from the liquid phase. The observation of crystalline solid solutions strengthens the hypothesis that the solid-state behavior of oxide **2a** has a clear-cut structural basis, rooted in its odd shape and inability to avoid suboptimal intermolecular interactions. As a result, its crystallization is prone to errors in which molecules of oxide **2a** are replaced by other compounds. A particularly attractive substitute is phosphangulene itself, which is identical in symmetry, topologically related, and smaller.

When isostructural compounds cocrystallize, the unit cell parameters typically vary linearly as the ratio of the components changes. This relationship, which is known as Vegard's law,^{37–39} unexpectedly also describes the behavior of mixtures of phosphangulene and oxide **2a**, even though they are far from isostructural. Figure 26 shows that the volume of the unit cell measured for single crystals of polymorph C of oxide **2a** decreases linearly as the amount of incorporated phosphangulene increases.

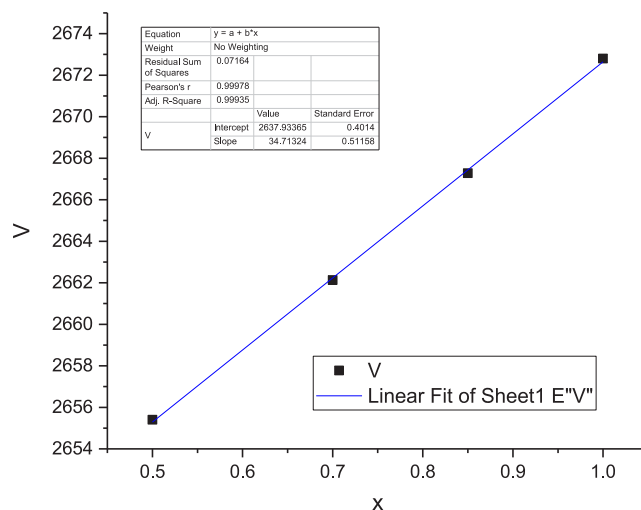


Figure 26. Graph showing that the unit cell volume V (in \AA^3) measured for single crystals of polymorph C of oxide **2a** decreases linearly as the molar fraction ($1 - \chi$) of incorporated phosphangulene increases.

The rapid high-fidelity crystallization of phosphangulene differs sharply from the promiscuous behavior of oxide **2a**. The contrast is an impressive example of how patterns of molecular organization can be altered substantially by simple structural modifications. The ability of oxide **2a** to include phosphangulene over a wide range of compositions is noteworthy because crystals of the pure components are not isostructural, or even structurally similar. The special tendency of oxide **2a** to form solid solutions appears to have the same origin as its high degree of polymorphism; specifically, the awkward shape inhibits effective packing, weakens intermolecular interactions, and broadens the opportunities to produce crystals in which the orientation and even the identity of

adjacent molecules can be varied without imposing a significant energetic penalty.

These conclusions are reinforced by the results of related experiments. For example, crystallization of equimolar mixtures of oxide **2a** and sulfide **2b** from CH₂Cl₂/hexane yielded crystals of oxide **2a** incorporating approximately 28% of sulfide **2b**. This surprising observation reveals that packing in the lattice of oxide **2a** is so susceptible to variations that sulfide **2b** can be accommodated, even though it is a larger molecule. Remarkably, examination of multiple mixed crystals showed that they all had similar compositions but formed two different structures. One corresponded to known polymorph A of oxide **2a** (monoclinic $P2_1/n$), but the other appears to be a new polymorph of oxide **2a** (monoclinic $P2_1/c$) that we have not yet been able to prepare in pure form. This observation suggests that further study of oxide **2a** will yield more polymorphs, beyond the five forms A–E already characterized in detail. Moreover, the promiscuous formation of mixed crystals is not a phenomenon limited to a single polymorph but rather is a more general consequence of the peculiar structural features of chalcogenides **2a–c**. The finding that oxide **2a** can be induced to crystallize in new ways by traces of additives provides further evidence that its molecular organization can be altered with unusual facility.

Chalcogenides **2a–c** also readily form pseudo-polymorphs incorporating molecules of various solvents, as well as cocrystals with diverse partners.⁴⁰ We have found that particularly suitable partners are fullerenes such as C₆₀ and C₇₀, which have convex surfaces that are topologically and electronically complementary to the concave faces of phosphangulene and its derivatives.^{40–43} The related propensity of triphenylphosphine oxide to cocrystallize with many partners has been noted in previous work and attributed in part to a strong capacity to accept hydrogen bonds.⁴⁴ Phosphangulene oxide (**2a**) promises to be an even more effective agent for promoting cocrystallizations, because it cannot crystallize effectively by itself in ways that properly exploit its latent ability to form hydrogen bonds and other interactions.

CONCLUSIONS

The distinctive conical shape of phosphangulene allows efficient molecular packing and helps direct crystallization by favoring the formation of π -stacks. As confirmed earlier by Krebs, Yamamura, and their co-workers, this preferred mode of association can be foiled by converting phosphangulene into the corresponding oxide **2a**, sulfide **2b**, or selenide **2c**. Only one atom is added, but molecular packing is altered profoundly. The shape of chalcogenides **2a–c** consistently disfavors efficient stacking and forces crystallization to occur in other ways. Detailed structural analysis of multiple polymorphs shows that none of the alternatives is particularly favorable, and the frequency of large intermolecular separations is always abnormally high. Chalcogenides **2a–c** are structurally unable to exploit the full potential of their constituent atoms to engage in stabilizing intermolecular contacts. A high degree of polymorphism is favored because various structural alterations can be accommodated without incurring significant energetic penalties, and the unit cells and asymmetric units of crystals must typically include large numbers of molecules to allow acceptable packing to be achieved.

Phosphangulene chalcogenides **2a–c** are richly polymorphic despite having little conformational flexibility. Statistical analysis of the CSD has established that molecular compounds

exhibit polymorphism in only about 37% of the single-component crystals examined;³⁰ moreover, only two inflexible compounds in the entire CSD (0.0002%) are known to exist in more than four polymorphic forms. As a result, the consistently unusual behavior of all three compounds **2a–c** is statistically improbable and refutes the notion that there are no correlations between molecular structure and high levels of polymorphism.

Our work builds on earlier investigations of phosphangulene and its derivatives but extends these previous studies in unexpected ways. Our observations reveal that the behavior of the compounds is not merely a curiosity, but rather a source of broadly useful new understanding of molecular crystallization overlooked in earlier work. Phosphangulene and its chalcogenides may appear to be exotic compounds, but they are not odd exceptions to normal molecular behavior. In fact, the series of compounds is aptly chosen to help reveal how molecular organization can be altered and controlled. Crystallization is an undeniably complex phenomenon, but our findings confirm that it is not futile to seek to identify specific structural features that underlie particular solid-state behavior. The approach used in our study of phosphangulene and its chalcogenides is based on purposeful interference with established patterns of crystallization, followed by extensive analysis of the consequences. Our results confirm that the approach is an effective way to probe the origins of molecular organization and to engineer materials with useful properties that arise predictably from structural features present in the individual molecular components.

Our results underscore the shortcomings of efforts to understand molecular crystallization based solely on statistical analyses of the CSD and other structural databases. Previous surveys have failed to identify any specific molecular features that predictably underlie high levels of polymorphism. Reported structures with high values of Z/Z' are also diverse, although certain organizing principles have been identified.²⁰ However, the guidelines are far too vague to allow confident extrapolation from the behavior of one compound to that of an analogue. We are not aware of any previous study in which the origin of high polymorphism and elevated values of Z/Z' has been traced back to specific structural features in a set of compounds, in the way that we have probed the behavior of phosphangulene chalcogenides **2a–c**. Moreover, the correlation we observe between molecular structure and crystalline organization is tight, allowing key features of the solid-state behavior of the entire set of compounds to be predicted with confidence, on the basis of the properties of a single example. This has not been achieved in previous efforts to understand the origin of polymorphism and elevated values of Z/Z' . Analyses of large databases are valuable tools for discovery, but they must be complemented by parallel experimental studies, using molecules purposefully devised to reveal and test principles of organization in crystals. Mining databases, however large, cannot yet replace sound chemical intuition as a way to locate promising areas for exploration within the infinite realm of molecular structures.

EXPERIMENTAL SECTION

All reagents and solvents were obtained from commercial sources and used without further purification unless otherwise indicated. Phosphangulene and chalcogenides **2a–c** were prepared by modifications of published procedures, as described below.^{1,7,13}

2-(3-Fluorophenoxy)tetrahydro-2H-pyran (4). To a stirred solution of pyridinium *p*-toluenesulfonate (0.305 g, 1.39 mmol) in 3,4-dihydro-2H-pyran (50 mL) was slowly added 3-fluorophenol (12.5 mL, 138 mmol) at 25 °C under N₂. After 30 min, the resulting mixture was concentrated by evaporating volatile components under reduced pressure, and ethyl acetate (200 mL) was added to the residue. The organic phase was washed with saturated aqueous NaHCO₃ (200 mL), water (200 mL), and brine (200 mL). The washed solution was then dried over Na₂SO₄ and filtered. Evaporation of volatiles under reduced pressure left an oily residue that was purified by flash chromatography (hexane, silica gel) to afford ether 4 as a colorless solid (21.6 g, 110 mmol, 79%). The ¹H and ¹³C NMR spectra matched those reported previously.¹

Tris[2-fluoro-6-(tetrahydro-2H-pyran-2-yloxy)phenyl]-phosphine (5). A stirred solution of ether 4 (20.7 g, 105 mmol) in dry THF (320 mL) was cooled to −85 °C under N₂ and treated dropwise with a solution of *n*-BuLi (42 mL, 2.5 M in hexane, 110 mmol) during 15 min. After 1 h at −85 °C, freshly distilled PBr₃ (9.23 g, 34.1 mmol) was added dropwise during 10 min. The resulting mixture was stirred for 2.5 h at −85 °C, then MeOH (5.5 mL) was added, and the temperature was allowed to rise to 25 °C. The quenched mixture was poured into brine (300 mL), and the mixture was extracted with diethyl ether (3 × 200 mL). The combined extracts were dried over Na₂SO₄ and filtered. Evaporation of volatiles under reduced pressure left a residue of solid, which was purified by trituration with boiling MeOH or by recrystallization from a boiling mixture of MeOH (1 L) and CHCl₃ (50–100 mL). The resulting solid was washed with MeOH and dried under vacuum to give phosphine 5 as a colorless solid (15.6 g, 25.3 mmol, 74%). The ¹H and ¹³C NMR spectra matched those reported previously.¹

2,2,2'-Phosphinetriyltris(3-fluorophenol) (6). Phosphine 5 (8.00 g, 13.0 mmol) was suspended in N₂-sparged MeOH (800 mL), and 36% aqueous HCl (16 mL, 190 mmol) was added. The mixture was stirred at 25 °C under N₂ until a solution was formed (about 1–1.5 h), and then volatile components were removed by evaporation under reduced pressure. The residue was dissolved in N₂-sparged CHCl₃ (300 mL), and N₂-sparged aqueous NaHCO₃ (1 N, 300 mL) was added. The two phases were vigorously stirred for 2 h under N₂ and then separated. The aqueous phase was extracted with diethyl ether (2 × 100 mL), and the combined organic phases were dried over Na₂SO₄ and filtered. Volatiles were removed by evaporation under reduced pressure, and the residue was then dissolved in boiling toluene (about 125 mL). Subsequent careful addition of heptane (200 mL) caused a colorless solid to precipitate. The resulting suspension was kept overnight at −25 °C to induce further precipitation. The product was separated by filtration, washed with hexane, and dried under vacuum to afford phosphine 6 as a colorless solid (4.31 g, 11.8 mmol, 91%). The ¹H and ¹³C NMR spectra matched those reported previously.¹

Phosphangulene (1). Under dry N₂, a mixture of phosphine 6 (1.82 g, 5.00 mmol), Cs₂CO₃ (12.2 g, 37.4 mmol), and CuI (0.0952 g, 0.500 mmol) was treated with dry DMF (75 mL) and freshly distilled tetramethylethylenediamine (TMEDA; 38 μL, 0.25 mmol). The mixture was heated at reflux for 2 days and then allowed to cool. Water was added until no more precipitate was formed. The solid was separated by filtration, washed thoroughly with water, and dried under vacuum at 25 °C. Decolorization could be achieved by dissolving the solid in CH₂Cl₂ and passing the solution through a pad of silica. This yielded phosphangulene (1) as a colorless solid (0.850 g, 2.79 mmol, 56%). The ¹H and ¹³C NMR spectra matched those reported previously.¹

Phosphangulene Oxide (2a). A solution of phosphangulene (1; 304 mg, 1.00 mmol) in CHCl₃ (8 mL) was treated with 30% aqueous hydrogen peroxide (10 mL), and the mixture was stirred vigorously at 25 °C for 12 h. The phases were separated, and the organic phase was dried over sodium sulfate and filtered. Removal of volatiles by evaporation under reduced pressure left a residue that was recrystallized from anhydrous ethanol to afford phosphangulene oxide (2a) as a colorless solid (307 mg, 0.959 mmol, 96%). The ¹H and ¹³C NMR spectra matched those reported previously.⁷

Phosphangulene Sulfide (2b). A solution of phosphangulene (1; 304 mg, 1.00 mmol) in *p*-xylene (3 mL) was sparged with N₂, and elemental sulfur was added (48.1 mg, 1.50 mmol). The resulting suspension was stirred and heated at reflux for 12 h. Volatiles were then removed by evaporation under reduced pressure, and the residue was purified by elution with hexane through a short column of silica. Crystallization of the product from anhydrous ethanol afforded phosphangulene sulfide (2b) as a colorless solid (259 mg, 0.770 mmol, 77%). The ¹H and ¹³C NMR spectra matched those reported previously.⁷

Phosphangulene Selenide (2c). A solution of phosphangulene (1; 304 mg, 1.00 mmol) in *p*-xylene (3 mL) was sparged with N₂, and elemental selenium was added (118 mg, 1.50 mmol). The resulting suspension was stirred and heated at reflux for 12 h. Volatiles were then removed by evaporation under reduced pressure, and the residue was purified by elution with hexane through a short column of silica. Crystallization of the product from anhydrous ethanol afforded phosphangulene selenide (2c) as a colorless solid (283 mg, 0.738 mmol, 74%). The ¹H and ¹³C NMR spectra matched those reported previously.⁷

■ ASSOCIATED CONTENT

📄 Supporting Information

The Supporting Information is available free of charge on the ACS Publications website at DOI: 10.1021/acs.cgd.9b00907.

Supplementary two-dimensional fingerprint plots of Hirshfeld surfaces and additional crystallographic details, including ORTEP drawings (PDF)

Accession Codes

CCDC 1912956–1912970 contain the supplementary crystallographic data for this paper. These data can be obtained free of charge via www.ccdc.cam.ac.uk/data_request/cif, or by emailing data_request@ccdc.cam.ac.uk, or by contacting The Cambridge Crystallographic Data Centre, 12 Union Road, Cambridge CB2 1EZ, UK; fax: +44 1223 336033.

■ AUTHOR INFORMATION

Corresponding Author

*E-mail: james.d.wuest@umontreal.ca.

ORCID

Thierry Maris: 0000-0001-9731-4046

James D. Wuest: 0000-0003-1847-6923

Notes

The authors declare no competing financial interest.

■ ACKNOWLEDGMENTS

We are grateful to the Natural Sciences and Engineering Research Council of Canada, the Ministère de l'Éducation du Québec, the Canada Foundation for Innovation, the Canada Research Chairs Program, and Université de Montréal for financial support.

■ DEDICATION

Dedicated to the memory of the late Joel Bernstein, whose deep understanding of molecular solids and infectious enthusiasm made him a valued friend and colleague.

■ REFERENCES

(1) Krebs, F. C.; Larsen, P. S.; Larsen, J.; Jacobsen, C. S.; Boutton, C.; Thorup, N. Synthesis, Structure, and Properties of 4,8,12-Trioxa-12c-phospha-4,8,12,12c-tetrahydrodibenzo[*cd,mm*]pyrene, a Molecular Pyroelectric. *J. Am. Chem. Soc.* **1997**, *119*, 1208–1216.

- (2) Carlson, R. R.; Meek, D. W. Dipole Moments of Several Tertiary Phosphine Oxides, Sulfides, and Selenides and of Some Tertiary Arsine Oxides and Sulfides. *Inorg. Chem.* **1974**, *13*, 1741–1747.
- (3) Cumper, C. W. N.; Foxton, A. A.; Read, J.; Vogel, A. I. Physical Properties and Chemical Constitution. Part XXXIX. The Electric Dipole Moments of Some Tri-*n*-alkylphosphines, of Triphenylphosphine, and of their Oxides. *J. Chem. Soc.* **1964**, 430–434.
- (4) Madsen, G. K. H.; Krebs, F. C.; Lebech, B.; Larsen, F. K. Evaluation of the Solid State Dipole Moment and Pyroelectric Coefficient of Phosphangulene by Multipolar Modeling of X-ray Structure Factors. *Chem. - Eur. J.* **2000**, *6*, 1797–1804.
- (5) Hirshfeld surfaces and two-dimensional fingerprint plots were generated by using CrystalExplorer17. Turner, M. J.; McKinnon, J. J.; Wolff, S. K.; Grimwood, D. J.; Spackman, P. R.; Jayatilaka, D.; Spackman, M. A. *Crystal Explorer17*; University of Western Australia, 2017.
- (6) McKinnon, J. J.; Spackman, M. A.; Mitchell, A. S. Novel Tools for Visualizing and Exploring Intermolecular Interactions in Molecular Crystals. *Acta Crystallogr., Sect. B: Struct. Sci.* **2004**, *60*, 627–668.
- (7) Yamamura, M.; Nabeshima, T. Relationship between the Bowl-Shaped Geometry of Phosphangulene and an Axial Group on the Phosphorus Atom. *Bull. Chem. Soc. Jpn.* **2016**, *89*, 42–49.
- (8) Maly, K. E.; Gagnon, E.; Wuest, J. D. Engineering Molecular Crystals with Abnormally Weak Cohesion. *Chem. Commun.* **2011**, 47, 5163–5165.
- (9) Gagnon, E.; Halperin, S. D.; Métivaud, V.; Maly, K. E.; Wuest, J. D. Tampering with Molecular Cohesion in Crystals of Hexaphenylbenzenes. *J. Org. Chem.* **2010**, *75*, 399–406.
- (10) Zhou, H.; Dang, H.; Yi, J.-H.; Nanci, A.; Rochefort, A.; Wuest, J. D. Frustrated 2D Molecular Crystallization. *J. Am. Chem. Soc.* **2007**, *129*, 13774–13775.
- (11) Lebel, O.; Maris, T.; Perron, M.-È.; Demers, E.; Wuest, J. D. The Dark Side of Crystal Engineering: Creating Glasses from Small Symmetric Molecules that Form Multiple Hydrogen Bonds. *J. Am. Chem. Soc.* **2006**, *128*, 10372–10373.
- (12) Zhang, X.; Liu, F.; Wei, Z.; Wang, Z. Synthesis of Diaryl Ethers by CuI-Catalyzed C-O Bond Formation via Ullman Coupling: Assessing the Reactivity of Aryl Halides. *Lett. Org. Chem.* **2013**, *10*, 31–36.
- (13) Faldt, A.; Krebs, F. C.; Thorup, N. Synthesis, Structure and Properties of Various Molecules Based on the 4,8,12-Trioxa-4,8,12,12c-tetrahydrodibenzo[*cd,mm*]pyrene System with an Evaluation of the Effect Differing Molecular Substitution Patterns has on the Space Group Symmetry. *J. Chem. Soc., Perkin Trans. 2* **1997**, *2*, 2219–2227.
- (14) Eikeland, E.; Thomsen, M. K.; Overgaard, J.; Spackman, M. A.; Iversen, B. B. Intermolecular Interaction Energies in Hydroquinone Clathrates at High Pressure. *Cryst. Growth Des.* **2017**, *17*, 3834–3846.
- (15) Lee, J. J.; Fuller, R. O.; Sobolev, A. N.; Clausen, H. F.; Overgaard, J.; Koutsantonis, G. A.; Iversen, B. B.; Spackman, M. A. Temperature-Dependent Crystal Structure of the Isopropanol Clathrate of Dianin's Compound. *Chem. Commun.* **2011**, 47, 2029–2031.
- (16) Kooijman, H.; Spek, A. L.; van Bommel, K. J. C.; Verboom, W.; Reinhoudt, D. N. A Triclinic Modification of Triphenylphosphine. *Acta Crystallogr., Sect. C: Cryst. Struct. Commun.* **1998**, *54*, 1695–1698.
- (17) Brock, C. P.; Schweizer, W. B. Internal Molecular Motion of Triphenylphosphine Oxide: Analysis of Atomic Displacement Parameters for Orthorhombic and Monoclinic Crystal Modifications at 100 and 150 K. *J. Am. Chem. Soc.* **1985**, *107*, 6964–6970.
- (18) Views of the structures of other inequivalent molecules in the asymmetric unit are provided in the [Supporting Information](#).
- (19) Bernstein, J.; Davey, R. J.; Henck, J.-O. Concomitant Polymorphs. *Angew. Chem., Int. Ed.* **1999**, *38*, 3440–3461.
- (20) Brock, C. P. High-*Z'* Structures of Organic Molecules: Their Diversity and Organizing Principles. *Acta Crystallogr., Sect. B: Struct. Sci., Cryst. Eng. Mater.* **2016**, *72*, 807–821.
- (21) Steed, K. M.; Steed, J. W. Packing Problems: High *Z'* Crystal Structures and Their Relationship to Cocrystals, Inclusion Compounds, and Polymorphism. *Chem. Rev.* **2015**, *115*, 2895–2933.
- (22) Bernstein, J.; Dunitz, J. D.; Gavezzotti, A. Polymorphic Perversity: Crystal Structures with Many Symmetry-Independent Molecules in the Unit Cell. *Cryst. Growth Des.* **2008**, *8*, 2011–2018.
- (23) Thomas, S. P.; Spackman, P. R.; Jayatilaka, D.; Spackman, M. A. Accurate Lattice Energies for Molecular Crystals from Experimental Crystal Structures. *J. Chem. Theory Comput.* **2018**, *14*, 1614–1623.
- (24) Zeidan, T. A.; Trotta, J. T.; Tilak, P. A.; Oliveira, M. A.; Chiarella, R. A.; Foxman, B. M.; Almarsson, O.; Hickey, M. B. An Unprecedented Case of Dodecamorphism: The Twelfth Polymorph of Aripiprazole Formed by Seeding with its Active Metabolite. *CrystEngComm* **2016**, *18*, 1486–1488.
- (25) Gnutzmann, T.; Thi, Y. N.; Rademann, K.; Emmerling, F. Solvent-Triggered Crystallization of Polymorphs Studied in Situ. *Cryst. Growth Des.* **2014**, *14*, 6445–6450.
- (26) López-Mejías, V.; Kampf, J. W.; Matzger, A. J. Nonamorphism in Flufenamic Acid and a New Record for a Polymorphic Structure with Solved Structures. *J. Am. Chem. Soc.* **2012**, *134*, 9872–9875.
- (27) Yu, L. Polymorphism in Molecular Solids: An Extraordinary System of Red, Orange, and Yellow Crystals. *Acc. Chem. Res.* **2010**, *43*, 1257–1266.
- (28) Brás, E. M.; Henriques, M. S. C.; Paixão, J. A.; Fausto, R. High *Z'* Crystal Structure of a New Polymorph of a Thioimidazole Disulfide: Importance of Conformational Flexibility. *Cryst. Growth Des.* **2018**, *18*, 4167–4173.
- (29) Kersten, K.; Kaur, R.; Matzger, A. Survey and Analysis of Crystal Polymorphism in Organic Structures. *IUCr* **2018**, *5*, 124–129.
- (30) Cruz-Cabeza, A. J.; Reutzel-Edens, S. M.; Bernstein, J. Facts and Fictions about Polymorphism. *Chem. Soc. Rev.* **2015**, *44*, 8619–8635.
- (31) McCrone, W. C. In *Polymorphism in Physics and Chemistry of the Organic Solid State*; Fox, D., Labes, M. M., Weissenberg, A., Eds.; Interscience: New York, 1965; Vol. II, pp 726.
- (32) Gavezzotti, A. Structure and Energy in Organic Crystals with Two Molecules in the Asymmetric Unit: Causality or Chance? *CrystEngComm* **2008**, *10*, 389–398.
- (33) Knapp, C.; Lork, E.; Gupta, K.; Mews, R. Structure Investigations on 4-Halo-1,2,3,5-dithiadiazolyl Radicals XCNSN* (X = F, Cl, Br): The Shortest Intradimer S...S Distance in Dithiadiazolyl Dimers. *Z. Anorg. Allg. Chem.* **2005**, *631*, 1640–1644.
- (34) Clarke, C. S.; Pascu, S. I.; Rawson, J. M. Further Studies on the Polymorphic Dithiadiazolyl Radical, ClCNSN. *CrystEngComm* **2004**, *6*, 79–82.
- (35) Cheuk, D.; Khamar, D.; McArdle, P.; Rasmuson, Å. C. Solid Forms, Crystal Habits, and Solubility of Danthron. *J. Chem. Eng. Data* **2015**, *60*, 2110–2118.
- (36) Rohl, A. L.; Moret, M.; Kaminsky, W.; Claborn, K.; McKinnon, J. J.; Kahr, B. Hirshfeld Surfaces Identify Inadequacies in Computations of Intermolecular Interactions in Crystals: Pentamorphic 1,8-Dihydroxyanthraquinone. *Cryst. Growth Des.* **2008**, *8*, 4517–4525.
- (37) Lusi, M. Engineering Crystal Properties through Solid Solutions. *Cryst. Growth Des.* **2018**, *18*, 3704–3712.
- (38) Vegard, L. Die Konstitution der Mischkristalle und die Raumfüllung der Atome. *Eur. Phys. J. A* **1921**, *5*, 17–26.
- (39) Vegard, L.; Shelderup, H. Die Konstitution der Mischkristalle. *Phys. Z.* **1917**, *18*, 93–96.
- (40) Heskia, A.; Maris, T.; Wuest, J. D. Putting Fullerenes in Their Place: Cocrystallizing C₆₀ and C₇₀ with Phosphangulene Chalcogenides. *Cryst. Growth Des.* **2019**, *19*, in press. DOI: 10.1021/acs.cgd.9b00954.
- (41) Yamamura, M.; Hongo, D.; Nabeshima, T. Twofold Fused Concave Hosts Containing Two Phosphorus Atoms: Modules for the Sandwich-Type Encapsulation of Fullerenes in Variable Cavities. *Chem. Sci.* **2015**, *6*, 6373–6378.

(42) Yamamura, M.; Sukegawa, K.; Nabeshima, T. Tuning the Depth of Bowl-Shaped Phosphine Hosts: Capsule and Pseudo-Cage Architectures in Host-Guest Complexes with C₆₀ Fullerene. *Chem. Commun.* **2015**, *51*, 12080–12083.

(43) Yamamura, M.; Saito, T.; Nabeshima, T. Phosphorus-Containing Chiral Molecule for Fullerene Recognition Based on Concave/Convex Interaction. *J. Am. Chem. Soc.* **2014**, *136*, 14299–14306.

(44) Etter, M. C.; Baures, P. W. Triphenylphosphine Oxide as a Crystallization Aid. *J. Am. Chem. Soc.* **1988**, *110*, 639–640.